Dynamics of viscous fingers and threshold instability

H. Guo
Center for the Physics of Materials and Department of Physics, Rutherford Building, McGill University, 3600 rue Universite, Montreal, Quebec, Canada H3A 2T8

Daniel C. Hong
Department of Physics and Polymers Interface Center, Lehigh University, Bethlehem, Pennsylvania 18015

Douglas A. Kurtze
Department of Physics, North Dakota State University, Fargo, North Dakota 58105-5566
(Received 24 August 1994)

We present a detailed weakly nonlinear analysis, along with a solvability analysis, of an instability in viscous fingering which we term the surface-tension-driven instability. This instability occurs when the surface tension is modified in proportion to the local curvature. It is an intrinsically nonlinear instability which always requires a finite-amplitude perturbation to trigger it. It is also distinctively different from those arising via subcritical bifurcation. Numerical simulations reveal that this instability leads to spiky cellular patterns and may suggest a possibility of leading to a finite time singularity.

PACS number(s): 47.20.Dr, 47.20.Ky, 47.55.Kf, 02.90.+p

I. INTRODUCTION

The viscous fingering instability [1] which occurs when a less viscous fluid pushes a fluid of high viscosity has continued to play a major role in both the scientific and industrial communities. On the practical level, it has important applications in a wide range of interdisciplinary fields, ranging through fluid flow in porous media [2–5], dendritic solidification [6], directional viscous fingering [7, 8], colloidal particle aggregation [9, 10], electrochemical deposition [11], surface growth [12], and oil recovery [13]. In addition, since the flow in a Hele-Shaw cell is simple and laminar, fingering experiments have been conducted with polymeric solutions in the hope of gaining useful insight into the role of polymers in flow phenomena, such as turbulent drag reduction [14]. Moreover, recent studies have revealed that there exist close similarities between the fingering instability and material failures [15–18]. On the scientific level, the goal would be to find some of the universal features (if any) common to many nonlinear phenomenologies by studying simple systems like viscous fingering. Indeed, extensive studies over the past several years have revealed that the "solvability" mechanism by which the finger width is selected [19] is identical to that in dendritic solidification [6], as well as in other similar pattern forming systems such as rising bubbles [20] and possibly directional solidification [21]. In addition, the evolution of the front in the fingering problem has been shown to have similarity solutions, and the critical exponents associated with these solutions have been computed numerically for the fingering problem [22, 23] and analytically for explosive crystallization [23].

In spite of much study, however, the analytic structure of the dynamics of the fingering instability remains poorly understood, being largely limited to the level of linear analysis [1, 6]. It is doubtless clear that one must carry out rigorous nonlinear analysis in order to gain insight into the dynamical process of fingering. Yet much of the theoretical study thus far has concentrated on steady-state patterns [24, 25] and the selection of finger widths [19], primarily by numerically solving the steady-state integro-differential equation. The purpose of this paper is to go one step farther and carry out a nonlinear bifurcation analysis. The surprising result of this investigation is the discovery of an intrinsically nonlinear instability termed here the surface-tension-driven instability [26]. Unlike linear instabilities such as the Mullins-Sekerka instability [27] in solidification, the Saffman-Taylor instability in viscous fingers [28], and the convective instability in the Rayleigh-Bénard problem [29], which can be triggered by infinitesimal perturbations, this instability always requires a perturbation whose amplitude exceeds a finite threshold. To the best of our knowledge, this is the first time that such an intrinsically nonlinear instability has been discovered.

This new instability also differs in a crucial way from the finite amplitude instability associated with a subcritical bifurcation. In the latter [30, 31], there is generally a control parameter, say β, with a critical value β_c beyond which a linear instability sets in. In these cases, nonlinear analysis reveals a finite amplitude instability when β is below β_c, with a threshold amplitude that vanishes as β reaches critical. Such an instability, however, is still *linear*, in the sense that its existence can be detected by linear analysis; nonlinear analysis is needed only to show that it persists as a finite amplitude instability even when the interface is stable against infinitesimal perturbations. On the other hand, the threshold instability to be presented below is intrinsically nonlinear. Unlike the subcritical bifurcation this instability has always a

nonzero threshold amplitude. Thus a simple linear analysis will miss it completely. As the control parameter is increased, the threshold amplitude becomes smaller, approaching but never reaching zero as the control parameter approaches infinity. Thus the threshold amplitude is always finite — the instability is never a linear one.

In the next section, we present the model equations that describe viscous fingering in systems with a surfactant. Section III shows that the linear stability analysis of the flat front is unaffected by the presence of a surfactant. In Sec. IV, we show that the surfactant can lead to narrow fingers in the case of less viscous fluid pushing more viscous one, or the control parameter $\beta < 0$, which will be defined shortly. Section V contains the weakly nonlinear analysis of the flat front in the case when a more viscous fluid pushes a less viscous one, and shows the possibility of a finite-amplitude instability with a vanishingly small threshold amplitude ($\beta > 0$). Section VI describes numerical integrations of the full model equations, and the results are discussed in Sec. VII.

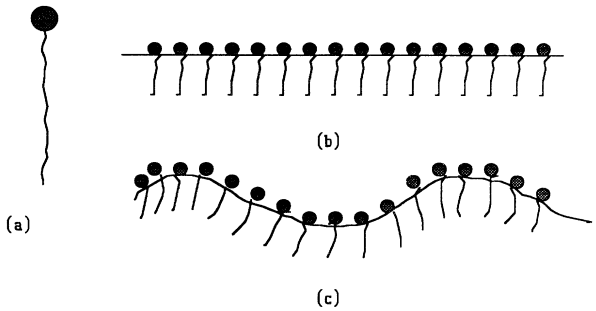

FIG. 1. (a) Polymers with hydrophobic tails (oil) and hydrophilic head group (water). (b) They rearrange themselves at the oil-water interface. (c) Due to entropic reasons, a region of positive curvature (bump) has slightly more polymers. U is the pushing velocity in the direction of the arrow. The threshold instability discussed in the text occurs when oil pushes water ($\beta > 0$).

II. MODEL EQUATIONS

The surface-tension-driven instability (hereafter termed SDI) results when surface tension is perturbed locally in proportion to local curvature. We note that the critical wavelength for the onset of instability in viscous fingering experiment (e.g., Ref. 1) is of order cm, so one might naively assume that observing the entropic effect due to polymers in the fingering instability in a Hele-Shaw cell might not be easy. However, as will be demonstrated later (i.e., Sec. V), the critical threshold amplitude to trigger SDI is of order q^{-1}, which is quite small in the presence of a cusplike singularity with enormously large curvature, $\kappa \approx q \gg 1$, (or extremely small radius of curvature, $r \approx q^{-1} \approx \kappa^{-1} \ll 1$) near the tip of the finger [see Fig. 5(b) and 5(c)]. Hence, while we do not have any conclusive evidence at this point, we expect that SDI can be observed experimentally with *polymeric* surfactants. SDI might be more relevant in studying the dynamics of the oil-water interface in a microemulsion, where the typical size of an immersed object is comparable to the size of the surfactants.

Now, consider polymeric surfactants with hydrophilic head A and hydrophobic tail B. When pushed together with water, the polymers will migrate toward the interface, where they quickly rearrange themselves to have their (hydrophilic) A and (hydrophobic) B groups pointing into the water and oil, respectively [Fig. 1(a)]. In order to study the polymers' effect on the fingering instability, one must first know how polymers residing at the interface modify the surface tension. This may be a complex function of the density and size of polymers, as well as the interaction among various types of molecules. Rigorous analysis will doubtless require careful study of the flow profile near the front in order to determine the density variations of polymers. As a first step, however, we recognize that it is entropically unfavorable to pack polymers in a region with a negative curvature, so the polymer concentration might be locally perturbed in proportion to the curvature. Further, if the polymer distribution relaxes on a time scale that is short compared to that of the interface motion, then the polymers will always be in local equilibrium and the surface tension, which depends on the concentration of polymers, will depend in turn on the local curvature. The surface tension is then modified to $\gamma(c) = \gamma_0 - \alpha c$, where $\alpha > 0$ and c is the local concentration of polymers. Note, however, that $c(\kappa) = c_0 - c_1\kappa$, where c_0 is the polymer concentration at the flat interface. Combining these two and ignoring higher order terms in κ, we find

$$\gamma(c) = \gamma + \beta\kappa, \tag{1}$$

with $\beta = \alpha c_1$. Note that β can be either positive or negative, depending on the sign of c_1. A negative value means that the surface tension is reduced in regions with positive curvature. This then tends to enhance the fingering instability. If the system is reversed, so that the more viscous fluid pushes the less viscous fluid, the β term helps suppress fingering, since the surface tension is increased when the more viscous fluid bulges into the less viscous fluid. On the other hand, a positive β tends to suppress the instability when the less viscous fluid pushes the more viscous one, but tends to produce fingering in the opposite situation.

The equations of motion for the fingering instability in a two-dimensional Hele-Shaw cell (Fig. 2) are

$$\nabla^2 P = 0 \tag{2a}$$

in the viscous fluid, with $\partial P/\partial x = 0$ at the impenetrable walls at $x = \pm 1$. At the interface between the fluids, we must have

$$P = -\gamma\kappa - \beta\kappa^2, \tag{2b}$$

$$v = -\nabla P. \tag{2c}$$

For convenience, the viscosity of the less viscous fluid has been set to zero, and we have chosen a time unit in which

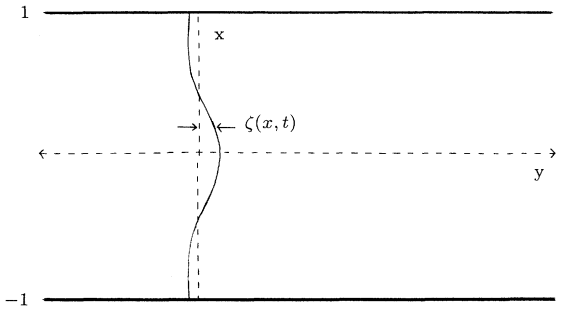

FIG. 2. Schematic diagram of a two-dimensional linear Hele-Shaw cell.

the steady-state front velocity is unity. The remainder of this paper is devoted to studying the effect of the new term $-\beta\kappa^2$ in (2b). We now briefly review the linear stability analysis [28].

III. LINEAR STABILITY ANALYSIS

Let the position of the initial flat interface be $y = 0$, and let it advance with unit velocity. Then at time t, the interface is at $y = t$ and the pressure field P is given by $P(x,y,t) = -(y-t)$. Consider a small perturbation of wave number k, growth rate ω, and amplitude δ_k. The interface position $\zeta(x,t)$ is given by

$$\zeta(x,t) \approx t + \delta_k e^{ikx+\omega t}. \tag{3}$$

The perturbed pressure field is

$$P(x,y,t) \approx -(y-t) + P_k e^{-k(y-t)+ikx+\omega t}. \tag{4}$$

Imposing the boundary condition (2c) gives the relation between P_k and δ_k,

$$k\,P_k = \omega\,\delta_k. \tag{5}$$

Finally, (2b) yields the relation between the growth rate ω and k,

$$\omega = k(1-\gamma k^2) = k[1-(k/k_c)^2], \tag{6}$$

where $k_c = \gamma^{-1/2}$. For $k < k_c$ we have $\omega > 0$, while for $k > k_c$, ω is negative. Note that at the level of linear analysis, it is impossible to detect the effect of β. We must go beyond linear analysis even to hint at the existence of a new instability caused by finite β.

IV. SOLVABILITY ANALYSIS

With $\beta < 0$, the fingering instability is enhanced and we expect narrow fingers to emerge when water pushes oil. We think this is the reason why narrow fingers were observed for the first few times only when the cell was washed with a soap full of surfactant molecules [32]. To be more specific, we now present the solvability analysis of the steady-state pattern selection given in Hong and Langer [19].

When the surface tension γ changes to $\gamma + \beta\kappa$ according to Eq. (1), the dimensionless parameter ν changes to $\nu(1-\epsilon\kappa/\nu)$, with κ the curvature. Hence the function $\Psi(\eta)$ in the solvability function Γ in Hong and Langer [19] will contain an additional term $1+\alpha(1+\beta^2\eta^2)/(1+\eta^2)^{3/2}$ in the denominator, with $\alpha = \beta\pi(1-\lambda)/\lambda^2\gamma = \epsilon(1-\lambda)^2 < 0$. Specifically, we find

$$\Psi(\eta) = 2i\beta^2 \int_0^\eta d\eta\,(1+i\eta)^{3/4}(1-i\eta)^{1/4} \times[1+\epsilon(1+\beta^2\eta^2)/(1+\eta^2)^{3/2}]^{-1/2} \times(1+\beta^2\eta^2)^{-1}, \tag{7}$$

and the solvability function Λ has the form

$$\Lambda \approx \int_{-\infty}^{\infty} d\eta\, f(\eta)\exp[\Psi(\eta)/\nu^{1/2}]. \tag{8}$$

Thus, in the limit $\nu \to 0$, Γ will be determined by the value of $\Psi(\eta)$ at its stationary point, namely $\eta = +i$. Note that with $\epsilon = 0$, $\Psi(\eta)$ has branch points at $z = \pm i$ and $z_b = \pm i/\beta \approx \pm i[1-4(\lambda-1/2)]$. So for $\lambda < 1/2$ the branch cut runs from $+i$ to $+i\infty$ and the solvability function Γ has no zeros, while for $\lambda > 1/2$ we have $|z_b| < 1$ and so it lies below (above) $i(-i)$, creating a new logarithmic branch cut from $+i$ to $+z_b$. Consequently, the stationary point i should be interpreted as a complex conjugate pair and Γ will oscillate as discussed in Hong and Langer [19]. With $\epsilon \neq 0$, there is now a new branch point on the imaginary axis located at $z_b = i - i\delta/2$ with $\delta = [|\epsilon|(1-\beta^2)]^{2/3}$ (we only consider the upper branch) and the original branch cut from $+i\infty$ to i now extends to z_b. Thus the steepest descent contour that runs from $-\infty$ to i to $+\infty$ now must contain z_b. The stationary value at i now has both real and imaginary parts due to the new branch cut from i to z_b. In order to find the contribution from this new branch cut to Γ, we expand $\Psi(\eta)$ around i. Letting $\eta = i - i\delta/2$, we find

$$\Psi(\eta) \approx \Psi(i) + 2^{5/4}i\beta^2 \int_0^\omega d\omega \times \frac{\omega^{3/4}}{(1-\beta^2)[1-|\epsilon|(1-\beta^2)/\omega^{3/2}]^{1/2}}. \tag{9}$$

Thus, when the contour runs from $i-\Delta$ to z_b and back to $i+\Delta$ with $\Delta \to 0$, $\Psi(\eta)$ will gain an additional term coming precisely from the journey along the additional cut. Let us define the discontinuity $\mathrm{Im}[\Psi(i)]$ as a quantity

$$\mathrm{Im}[\Psi(\eta)] \approx \lim_{\Delta\to 0}[\Psi(i-\Delta) - \Psi(i+\Delta)], \tag{10}$$

which, in the limit $\Delta \ll 1$, is of the order of the integral on the left side of Eq. (9) with the upper limit $\omega \approx \Delta$, namely

$$\mathrm{Im}[\Psi(i)] \approx \frac{\beta^2 z_b^{7/4} z_b^{3/4}}{(1-\beta^2)[|\epsilon|(1-\beta^2)]^{1/2}}. \tag{11}$$

Hence, the solvability function Λ is now written as

$$\Lambda \approx \exp[\Psi(i)/\nu^{1/2}]\cos(\mathrm{Im}[(\Psi(i)]/\nu^{1/2}). \tag{12}$$

For $\mathrm{Im}[\Psi(i)] \ll \nu^{1/2}$, Λ will have no zeros, while for $\mathrm{Im}[\Psi(i)] \gg \nu^{1/2}$, the cosine function oscillates and pro-

duces many zeros and thus the solvability condition is satisfied. The pattern will be selected when $\mathrm{Im}[\Psi(i)] \approx \nu^{1/2}$. The crossover condition from non-oscillatory to oscillatory solutions sets the criterion for the selection mechanism, which is termed the "resolution criterion." This yields

$$\frac{\Delta^{5/2}}{\nu^{1/2}} \frac{\beta^2}{|\epsilon|^{1/2}(1-\beta^2)^{3/2}}. \tag{13}$$

Rearranging the terms, we thus find the following scaling relation among α, β and $\nu = \pi b^2\gamma/12UW^2(1-\lambda)^2$:

$$\nu/\lambda^4 \approx |\epsilon|^{7/3}(1-2\lambda)^{1/3}. \tag{14}$$

There is at least one experimental case where narrow fingers were observed with polymers or surfactants. In the experiment conducted by Kopf-Sill and Homsy [32], a Hele-Shaw cell was cleaned with a soap containing surfactant molecules. They then observed narrow fingers when water pushes oil but only for the first few runs, after which normal Saffman-Taylor fingers emerged. It is clear that in the first few runs after cleaning with soap, the surfactant molecules remaining in the cell are responsible for the appearance of narrow fingers. In this context, it might not be entirely unphysical to assume that the surfactant molecules caused the surface tension to modify in proportion to local curvature. However, it is possible that some other mechanism than what is considered in this section could be in action.

V. WEAKLY NONLINEAR ANALYSIS AND THE THRESHOLD INSTABILITY

We now turn our attention to the bifurcation analysis in the weakly nonlinear regime in the opposite case of oil pushing water ($\beta > 0$.) Note that since β enters through the κ^2 term in the pressure boundary condition (2b), it has no effect on the linear stability analysis and thus we must perform a nonlinear analysis. This can be done in a weakly nonlinear regime, in which the linear growth of the most unstable (or least stable) mode is small. The weakly nonlinear regime can be realized by making the critical wavelength $k_c = \gamma^{-1/2}$ only slightly larger than $\pi/2$, the smallest perturbation wave number allowed by the periodic boundary conditions. This can be accomplished by adjusting the surface tension γ via the overall polymer concentration. In this limit, the lowest mode should have the largest amplitude, and since its linear growth rate is small we expect this amplitude to saturate at a small value. We may then expand the interface position $\zeta(x,t)$ and the corresponding pressure field $P(x,y,t)$ in Fourier modes,

$$\zeta(x,t) = t + \sum_k \zeta_k(t)\cos k(x+1), \tag{15}$$

$$P(x,y,t) = -(y-t) + \sum_k P_k(t)e^{-k(y-t)} \times \cos k(x+1), \tag{16}$$

where the use of cosines respects the impenetrable boundary conditions at $x = \pm 1$; the allowed wave numbers are $k = n\pi$ with $n = 0, 1, 2, \ldots$. The expression (16) for the pressure automatically satisfies the Laplace's equation. By substituting these expansions into the boundary conditions (2b) and (2c) at the interface, we obtain equations of motion for the sets of coefficients ζ_k and P_k. This is carried out in the appendix.

In the weakly nonlinear regime, all the ζ_k should remain small, so we can expand in powers of the ζ_k to get an equation of motion for the ζ_k themselves. The (quite lengthy) algebra is outlined in the appendix. To third order, for $q \neq 0$, we obtain

$$\begin{aligned} q^{-1}\frac{d\zeta_q}{dt} = {} & (1-\gamma q^2)\zeta_q - \frac{1}{2}\beta\sum_k k^2\zeta_k[(q-k)^2(\zeta_{q-k}+\zeta_{k-q}) + (q+k)^2\zeta_{q+k}] + \sum_k k(1-\gamma k^2)\zeta_k\zeta_{q+k} \\ & + \frac{1}{2}\sum_{k,k'} k\zeta_{q+k}\zeta_{k'}[k'(1-\gamma k'^2) - \beta k'^2(k+k')^2]\zeta_{k+k'} + [k'(1-\gamma k'^2) - \beta k'^2(k-k')^2] \\ & \times(\zeta_{k-k'} + \zeta_{k'-k}) - \frac{1}{4}\sum_{k,k'} k^2(1-\gamma k^2)\zeta_k\zeta_{k'}(\zeta_{q+k+k'} + \zeta_{q+k-k'} + \zeta_{-q-k+k'}) \\ & + \frac{3}{4}\gamma\sum_{k,k'} k^2k'\zeta_k\zeta_{k'}[(q+k+k')\zeta_{q+k+k'} + (k'-k-q)(\zeta_{k'-k-q} + \zeta_{q+k-k'}) \\ & + (k'-k+q)(\zeta_{k'-k+q} + \zeta_{k-k'-q}) + (k'+k-q)(\zeta_{k'+k-q} + \zeta_{q-k-k'})]. \end{aligned} \tag{17}$$

In addition, we find that the average displacement of the interface relative to the flat front, ζ_0, is constant in time, while ζ_0 itself does not appear in the equations of motion for the ζ_k. This is true in general, not just in the weakly nonlinear approximation. Indeed, the contributions to the right-hand side of (17), which contain ζ_0, all cancel. Thus the average position of the interface neither affects nor is affected by the interface shape. This reflects the translational symmetry of the original problem.

If we allow only one mode, then (17) reduces to

$$d\zeta_q/dt = q(1-\gamma q^2)\zeta_q - \tfrac{1}{4}q^3(1-\tfrac{5}{2}\gamma q^2)\zeta_q^3, \tag{18}$$

so once again we find no β dependence. The effect of β shows up only if we take into account interactions among different modes.

We now truncate (17) to the lowest two modes and find the following dynamic equations:

$$d\zeta_q/dt = q(1-\gamma q^2)\zeta_q + q^2(1-\gamma q^2 - 4\beta q^3)\zeta_q\zeta_{2q} + q^3\left(\tfrac{5}{8}\gamma q^2 - \tfrac{1}{4}\right)\zeta_q^3 + q^3\left(\tfrac{13}{2}\gamma q^2 - \tfrac{1}{2} - 4\beta q^3\right)\zeta_q\zeta_{2q}^2, \quad (19a)$$

$$d\zeta_{2q}/dt = 2q(1-4\gamma q^2)\zeta_{2q} - \beta q^5\zeta_q^2 + q^3(7\gamma q^2 - 1)\zeta_q^2\zeta_{2q} + 2q^3(10\gamma q^2 - 1)\zeta_{2q}^3. \quad (19b)$$

One may carry out a bifurcation analysis for these equations. Nothing very interesting happens, except that the β term enhances the instability. New, more interesting phenomena, however, occur in the opposite configuration where the more viscous fluid pushes the less viscous one, the configuration that is always linearly stable. The amplitude equations for this situation can be obtained from (19) by replacing t, γ, and β by $-t$, $-\gamma$, and $-\beta$, respectively. This gives the following coupled nonlinear equations of motion for the two lowest modes:

$$\dot{x} = -(1+\Gamma)x - (1+\Gamma+3B)xy + (1+5\Gamma/2)x^3 + (1/2+13\Gamma/2-3B)xy^2, \quad (20a)$$

$$\dot{y} = -2(1+4\Gamma)y - 3Bx^2 + 4(1+4\Gamma)x^2y + 2(1+7\Gamma)y^3, \quad (20b)$$

where we have introduced new notations: $x = q\zeta_q/2$, $y = q\zeta_{2q}$, $B = 4\beta q^3/3$, $\Gamma = \gamma q^2 > 0$, and the overdot represents a rescaled time derivative, $q^{-1}d/dt$.

This pair of equations has a fixed point at $(x,y) = (0,0)$, which represents the flat interface solution. This fixed point is an attractor, as we can see easily from the fact that Γ is positive. There is also a pair of unstable fixed points at $(x,y) = (0,\pm\alpha)$ with $\alpha = [(1+4\Gamma)/(1+7\Gamma)]^{1/2}$. These fixed points are both unstable in the y direction. By linearizing about them, we find that the fixed point at $(0,-\alpha)$ is a repeller, while the one at $(0,\alpha)$ is a repeller for large Γ but a saddle for small Γ or large B.

In the usual fingering problem without surfactant, we have $B = 0$. For this case there can be as many as six fixed points. In addition to the three discussed above, there is one at $([2(1+\Gamma)/(2+5\Gamma)]^{1/2},0)$, and up to two at the solutions of

$$x^2 = \frac{2(1+\Gamma)(1+y) - (1+13\Gamma)y^2}{2+5\Gamma} = \frac{(1+4\Gamma) - (1+7\Gamma)y^2}{2(1+4\Gamma)}. \quad (21)$$

Linearizing about the fixed points, and numerical integration of the equations of motion, reveal the structure of the phase portrait of the system. For small Γ, there is one fixed point given by (21); it and the fixed point $(0,\alpha)$ are saddles while the other two (besides the origin) are repellers. The basin of the attractor at the origin is bounded by trajectories that run from the repellers to the saddles, as shown in Fig. 3(a). A bifurcation occurs

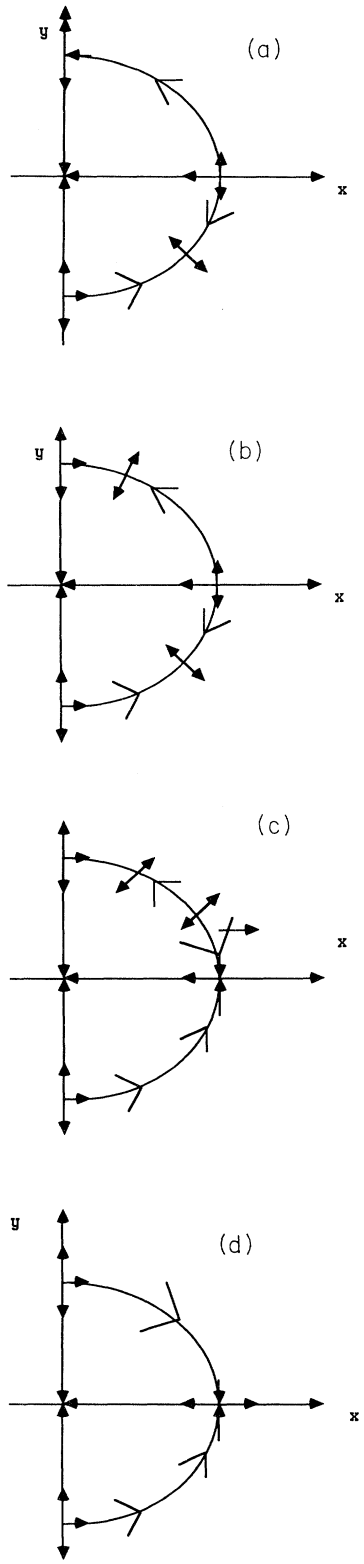

FIG. 3. Flow diagrams for the two mode approximation, Eq. (20). The plot is symmetric in x; only the positive-x half is shown. Fixed points are shown as black dots. The saddles and repellers mark the boundary of the basin of the attractor at the origin. (a) $0 < \Gamma < 0.608$, (b) $0.608 < \Gamma < 2$, (c) $2 < \Gamma < 3.314$, and (d) $3.314 < \Gamma$.

at $\Gamma = 0.608\,171\,691$ in which another solution of (21) appears in a pitchfork bifurcation with $(0,\alpha)$. The new fixed point is a saddle, while $(0,\alpha)$ becomes a repeller. At $\Gamma = 2$, the original solution of (21) and the fixed point on the x axis cross in a transcritical bifurcation; the former becomes a repeller and the latter a saddle. Finally, the two solutions of (21) merge and disappear in a saddle-node bifurcation at $\Gamma = 3.314\,287\,613$. The basic structure of the phase plane always remains the same, however, the fixed point at the origin is an attractor, and the stable manifolds of the saddle points delimit its basin of attraction. An initial state that is outside the basin follows a trajectory that takes it out to infinity, signaling the breakdown of the approximations that led to the evolution equations (20). The phase portraits for increasing Γ are shown in Fig. 3.

For finite B, the character of the phase portrait is quite similar to that for $B = 0$. The fixed point on the x axis and those given by (21) become the solutions of

$$x^2 = \frac{2(1+\Gamma)+2(1+\Gamma+3B)y-(1+13\Gamma-6B)y^2}{2+5\Gamma} = \frac{2(1+4\Gamma)y-2(1+7\Gamma)y^3}{-3B+4(1+4\Gamma)y}. \tag{22}$$

Cross multiplying gives a cubic in y, so there are at most three solutions. Bifurcations among these fixed points can occur when this cubic has multiple zeros, and bifurcations with the fixed points on the y axis can occur when (22) has solution with $x^2 = 0$. However, the picture of an attractor at the origin whose basin is bounded by the stable manifolds of saddles is maintained.

There is, however, an important *quantitative* change as B is increased. To see it, we examine the fixed points given by (22) in the limit $|B| \to \infty$. Cross multiplying and retaining only the highest powers of B in the coefficients of each power of y, we get

$$4(1+4\Gamma)y^3 - 3By^2 - 3By - (1+\Gamma) = 0. \tag{23}$$

To leading order in B, the three solution of this cubic are $3B/4(1+4\Gamma)$, -1, and $-(1+\Gamma)/3B$. The corresponding values of x^2 are $6By^2/(2+5\Gamma)$, $-2\Gamma/B$, and $2(1+\Gamma)(1+4\Gamma)/9B^2$, respectively; thus the first and third are fixed points for $B \to \infty$ and the second and third are fixed points for $B \to -\infty$. The phase portrait is sketched in Fig. 4. The important point here is the existence of the third fixed point (which turns out to be a saddle). The stable manifold of this saddle is part of the separatrix that delimits the basin of attraction of the flat-interface fixed point $(0,0)$. Thus we see that in the limit of large $|B|$, the flat interface is *linearly* stable, but a perturbation whose amplitude is only of order $|B|^{-1}$ is large enough to destroy it. This threshold, while nonzero, can be so small that the flat interface will be unstable for all practical purposes, even though linear stability analysis predicts it to be stable.

In this connection, it is useful to recall the definitions of the parameters Γ and B, namely γq^2 and $4\beta q^3/3$, respectively. We have found that for $|B| \gg \Gamma$, there is a finite-amplitude instability of the flat interface which is invisible to linear stability analysis, but whose threshold amplitude is only of order $\Gamma/|B|$, which is itself proportional to q^{-1}. Thus having surface tension change in proportion to the curvature of the interface can lead to a nonlinear instability against short-wavelength perturbations.

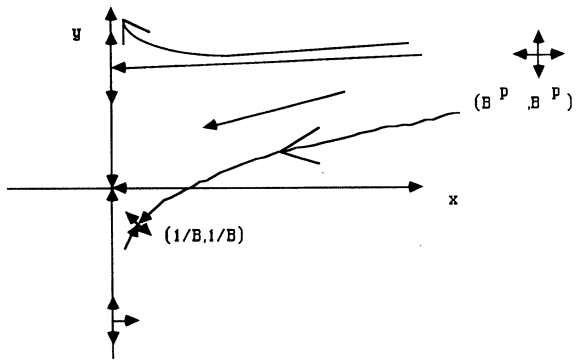

FIG. 4. Flow diagram with large B, as in Fig. 4. Note the shape of the basin boundary, and the fixed point near the origin. In the limit $B \to \infty$, the unstable fixed points are at $\sim (B, B^{3/2})$ and $\sim (1/B, 1/B)$, so the flat interface is unstable to finite but small amplitude perturbations.

VI. NUMERICAL TESTS

In order to test the predictions of the above two-mode analysis, we have carried out numerical integrations of the equations of motion (2). The numerical scheme is the same as in Refs. [22], [23], and [26], which we review very briefly for completeness.

Defining a velocity potential $\Phi \equiv \phi + Uy$ with $\phi \equiv b^2P/12\mu$ and $Y \equiv y - Ut$, and assuming $\mu_1 \approx 0$, Eq. (2) can be rewritten as

$$v_n' = -\hat{n}\nabla\Phi = -v_n + U\cos\theta, \tag{24a}$$

$$\Phi_s = \phi_s + Uy = -\gamma\kappa + U\zeta(x), \tag{24b}$$

$$\Phi \to 0 \quad \text{as} \quad Y \to \infty, \tag{24c}$$

$$\left.\frac{\partial\Phi}{\partial n}\right|_{wall} = 0, \tag{24d}$$

where θ is the angle between the interface normal and the $+y$ direction and $\zeta(x)$ is the y coordinate of the interface, i.e., it is the interface shape.

The last set of equations can be further reduced to a single equation for the interface shape via Green's theorem, using the two-dimensional Green's function which satisfies $\nabla^2 G = -\delta(\vec{r}-\vec{r}')$ and is periodic in the x direction,

$$G(x-x', y-y') = -\frac{1}{4\pi}\ln\left[\cosh\frac{2\pi|y-y'|}{W} - \cos\frac{2\pi|x-x'|}{W}\right]. \tag{25}$$

Using a contour that goes along the interface and around the cell walls, (24) is reduced to an integro-differential equation which we solve numerically,

$$-\frac{1}{2}\left[\gamma\kappa(s)-\frac{U}{2}\zeta(s)\right]+\int ds'\left[\gamma\kappa(s')-\frac{U}{2}\zeta(s')\right]\frac{\partial G(s,s')}{\partial n'}=\int ds'\,G(s,s')v_{n'}(s'), \quad (26)$$

where s and s' are contour variables along the interface and the integrations extend over the entire interface. From this equation, we obtain the normal velocity of the interface v_n if the interface shape $\zeta(x)$ is known. The interface is then moved forward in time by essentially solving $d\zeta/dt = v_n \cos\theta$. Thus given an initial interface shape, its time evolution can be obtained. Details of the numerical scheme can be found in Refs. [22] and [23].

As initial conditions, we perturb a flat interface by a sinusoidal function of a given wave number q; thus the initial shape of the interface is $\zeta(x) = A[\sin(2\pi qx/W) + \cos(2\pi qx/W)]$, where A is the amplitude of the perturbation. The time evolution of this perturbation is then followed by solving (26) iteratively. Recall that we are now pushing the less viscous fluid with the more viscous one, thus without the change in the Gibbs-Thomson relation, i.e., when $\beta = 0$, the interface is completely stable. However, with $\beta \neq 0$, our weakly nonlinear analysis has indicated the possibility of a new threshold instability taking place.

For fixed external parameters such as the pushing velocity and the surface tension, the interface is stable if the amplitude A of the initial perturbation is small. In Fig. 5(a) it is clear that a small amplitude perturbation indeed evolves to zero and eventually will become a simple flat shape. Increasing the amplitude with all other parameters fixed, the interface evolves into the shapes shown in Figs. 5(b) and 5(c), and is obviously unstable against forming cellular patterns. Note that the patterns are quite different from those seen in directional solidification in that the shape around the tip of each cell is quite spiky. Thus, as predicted by the analysis of the previous section, the instability indeed depends on the value of the perturbation amplitudes. The instability also depends on the value of the parameter β. Reducing β and keeping all other parameters as those of Fig. 5(c), the instability disappears as shown in Figs. 6(a) and 6(b). This is understandable since a finite amplitude perturbation is needed to trigger the instability and that amplitude depends on the values of β, as the flow diagram shows (see Fig. 4). Since the instability is controlled by the parameter $B \propto \beta q^3$, we expect that increasing the wave number q will also lead to instability with all other parameters fixed. This is distinctly different from the well-known Mullins-Sekerka instability where modes with large wave numbers are stable. Figure 7 shows the width of the interface, $Z(t) \equiv \sqrt{[\sum_i \zeta(x_i) - \zeta_0]^2/W^2}$, as a function of time for different q values. Here ζ_0 is the average position of the interface. For small q values, $Z(t)$ simply decreases to zero at large times, thus the interfaces are

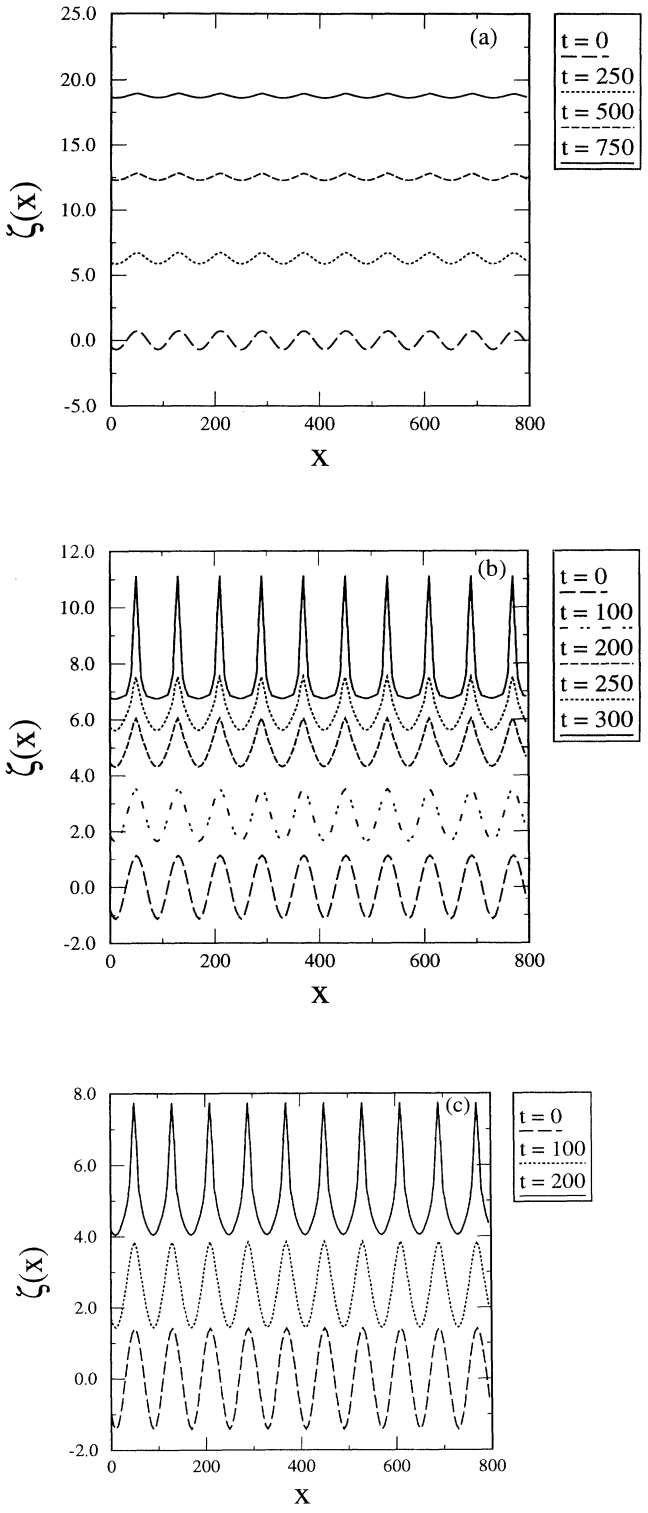

FIG. 5. Time evolution of the fluid interface shape. The parameters used here are: wave number $q = 10$, pushing velocity $U = -0.025$, surface tension $\gamma = 1.0$, $\beta = -400$. (a) The amplitude of the initial perturbation is $A = 0.5$. No instability is detected and the interface evolves to flat shape at large times; (b) $A = 0.8$, the interface is unstable; (c) $A = 1.0$, the interface is unstable.

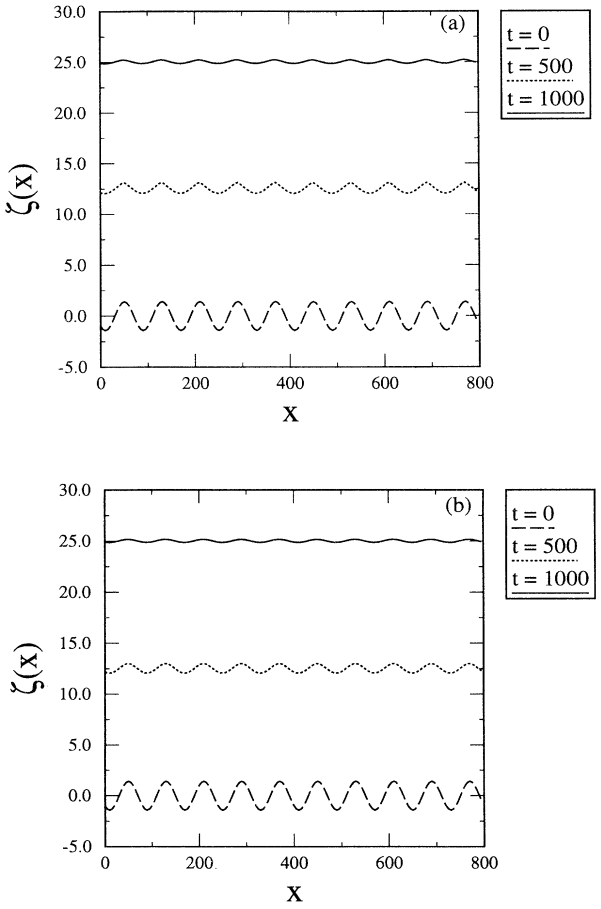

FIG. 6. Time evolution of the interface shapes as the value of the control parameter β is reduced. All the parameters are the same as those used to produce Fig. 6(c) except β: (a) $\beta = -200$; (b) $\beta = -100$. The interface becomes stable as the value of β is reduced.

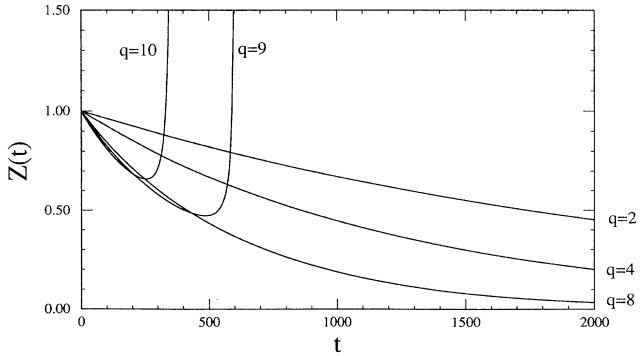

FIG. 7. Time evolution of the interface width defined as $Z(t) \equiv \sqrt{[\sum_i \zeta(x_i) - \zeta_0]^2/W^2}$ for different wave numbers q. Other parameters are the same as those for Fig. 6(c). Large q values lead to instability, as the width diverges in time.

flat at large times and the modes are stable. For large q values, $Z(t)$ diverges at large times signaling the onset of instability. These observations are in qualitative agreement with the results of the weakly nonlinear analysis. Finally, we note that the cellular patterns arising from the instability are due to changes in the surface tension, and thus we expect that any perturbation that changes the pressure boundary condition, like (1), could produce the same effect.

VII. DISCUSSION AND CONCLUSIONS

We now discuss a few cases where the observed instability might correspond to what has been discovered in this paper.

(a) Oil pushing air in a Hele-Shaw cell with a scratched plane: Maher [33] conducted a fingering experiment in a linear Hele-Shaw cell, on the bottom plate of which was created a square lattice by grooving it. Water pushing oil in the presence of a groove that provides anisotropy is well documented and well understood [34, 35]. However, the opposite case has never been studied. Maher observed that upon pushing oil into air, the interface becomes unstable and soon develops sharp cellular kinks much the same as shown in Fig. 5(b). While the cause of this instability is unclear at this moment, it is tempting to suggest that such instability might be triggered through the change in the boundary condition (2b). Work is in progress along this direction.

(b) Oil mixed with dye particles: Another experiment that came to our attention was the one done with oil mixed with dye particles. Couder [36] informed us that when he injected dye particles into the oil phase, he observed that the oil-pushing-water interface developed cellular patterns similar to that seen in Fig. 6(c). Here one might argue that the dye particles migrate toward the interface upon pushing. The region with positive curvature might contain slightly more dye particles because of two reasons: one is a simple entropic argument discussed in Sec. II and the other one is that the region with a positive curvature provides a comfortable valley for dye particles to aggregate, which decreases surface tension. Therefore, one might expect that the surface tension could be modified as in (2b).

(c) Recently, there have been considerable attempts to search for the finite time singularity in a simple flow such as an Eulerian flow [37] and Hele-Shaw flow [38]. We are tempted to view the development of sharp needlelike patterns seen in Fig. 5(c) as a possible indication leading to this direction, although we want to caution the reader not to be too optimistic. It is quite difficult even to study the long time dynamics of SDI instability, but we hope to present near future studies along this direction.

In conclusion, in this paper, we have considered dynamics of viscous fingering instability when surface tension is modified in proportion to local curvature. When a less viscous fluid pushes a more viscous one, this results in narrow fingers and we have presented the scaling relation between the control parameter β and dimensionless surface tension parameter ν and the finger width λ based on the solvability analysis. But the central result

of this work is the discovery of an instability, termed here surface-tension-driven nonlinear instability (SDI), in the opposite case when a more viscous fluid pushes a less viscous one. We have carried out detailed bifurcation analysis for such a case and shown in detail how one could miss the existence of such instability by a naive linear analysis. This is the first time to our knowledge, that such an intrinsically nonlinear instability has been discovered. We hope that our study might stimulate others to search for nonlinear instability in other pattern forming systems in the future.

ACKNOWLEDGMENTS

H.G. is supported by the Natural Sciences and Engineering Research Council of Canada and le Fonds pour la Formation des Chercheurs et l'Aide a la Recherche de la Province du Quebec. H.G. and D.C.H. are also supported by NATO exchange program. D.A.K. is supported by the National Science Foundation, through the EPSCoR program administered by ASEND in North Dakota, and by the National Aeronautics and Space Administration through the JOVE program at North Dakota State University. Part of the computation has been conducted on the Cornell National Supercomputer Facility. Polymers Interface Center at is supported by NSF-IUCRC program.

APPENDIX

In this appendix, we derive the amplitude equation (17). In a reference frame moving with the steady-state flat interface, the interface position $\zeta(y,t)$ can be written in terms of Fourier modes,

$$\zeta(y,t)=\sum_k \zeta_k(t)\cos k(y+1), \tag{A1}$$

and the pressure field, which satisfies Laplace's equation, is given by

$$P(x,y)=-x+\sum_k P_k(t)\exp(-kx)\cos k(y+1). \tag{A2}$$

In order to satisfy the impenetrable boundary conditions at $y=\pm 1$, the allowed wave numbers are $k=n\pi$ with $n=1,2,3,\ldots$.

The flux boundary condition (2c) at the interface can be written explicitly as

$$1+\frac{\partial\zeta}{\partial t}=\left[-\frac{\partial P}{\partial x}+\frac{\partial\zeta}{\partial y}\frac{\partial P}{\partial y}\right]_{x=\zeta}, \tag{A3}$$

inserting (A1) and (A2) and simplifying puts this in the form

$$\sum_k \frac{d\zeta_k}{dt}\cos k(y+1)=\sum_k P_k(t)\frac{\partial}{\partial y}\{\exp[-k\zeta(y)]\times\sin k(y+1)\}. \tag{A4}$$

Note that this implies that ζ_0 is constant in time, as seen by integrating from $y=-1$ to $y=1$. Multiplying by $\cos q(y+1)$ and integrating yields

$$\frac{d\zeta_q}{dt}=q\sum_k P_k(t)\int_{-1}^{1}\sin q(y+1)\exp[-k\zeta(y)]\times\sin k(y+1)\,dy. \tag{A5}$$

Note, from the appearance of $\sin k(y+1)$ in the integral that there is no contribution from $P_0(t)$ to the time evolution of the front. Equation (A5) is to be solved together with the pressure boundary condition (2b), which becomes

$$\sum_k P_k(t)\exp[-k\zeta(y)]\cos k(y+1)=\zeta-\gamma\kappa-\beta\kappa^2, \tag{A6}$$

or

$$\sum_k P_k(t)\int_{-1}^{1}\cos q(y+1)\exp[-k\zeta(y)]\cos k(y+1)\,dy=\zeta_q-\int_{-1}^{1}(\gamma\kappa+\beta\kappa^2)\cos q(y+1)\,dy. \tag{A7}$$

Note again that changing ζ_0 has no effect on the time evolution of the other modes. First, since each coefficient P_k only appears multiplied by $\exp(-k\zeta)$ in both (A5) and (A7), a change to ζ_0 can be absorbed into the P_k. Second, ζ_0 appears on the right side of (A7) only for $q=0$, where it affects only P_0; as we have seen, P_0 does not affect the time evolution of the interface.

In the weakly nonlinear regime, we can simplify equation (A5) and (A7) by expanding in powers of the coefficients ζ_k. First we will use (A7) to find the pressure coefficients P_k to second order. To this order, the curvature κ is just equal to $\partial^2\zeta/\partial y^2$. Substituting the expansion (A1) for ζ into (A7), expanding to second order, and evaluating the integrals gives

$$P_k=(1-\gamma k^2)\zeta_k-\frac{1}{2}\beta\sum_{k'}k'^2\zeta_{k'}[(k-k')^2\times(\zeta_{k-k'}+\zeta_{k'-k})+(k+k')^2\zeta_{k+k'}]+\frac{1}{2}\sum_{k'}k'P_{k'}(\zeta_{k+k'}+\zeta_{k-k'}+\zeta_{k'-k}). \tag{A8}$$

Iterating this expansion and rearranging terms finally gives

$$P_k=(1-\gamma k^2)\zeta_k-\frac{1}{2}\sum_{k'}\{[k'(1-\gamma k'^2)-\beta k'^2(k+k')^2]\times\zeta_{k'}\zeta_{k+k'}+[k'(1-\gamma k'^2)-\beta k'^2(k-k')^2]\zeta_{k'}\zeta_{k-k'}\}. \tag{A9}$$

The rest of the derivation consists of substituting this result into (A5), expanding to third order, and evaluating the integrals. This task becomes slightly less arduous, however, if instead of starting with (A5) itself we start by subtracting (A5) (divided by q) from (A7). This gives

$$\sum_k P_k\int_{-1}^{1}\exp[-k\zeta(y)]\cos(k+q)(y+1)\,dy=q^{-1}\frac{d\zeta_q}{dt}-\zeta_q+\int_{-1}^{1}(\gamma\kappa+\beta\kappa^2)\cos q(y+1)\,dy. \tag{A10}$$

Now substituting for P_k, expanding, evaluating the integrals over y, and rearranging yields Eq. (17) of the text.

[1] P.J. Saffman, J. Fluid Mech. **173**, 73 (1986); G.M. Homsy, Ann. Rev. Fluid Mech. **19**, 271 (1987); D. Bensimon, L. Kadanoff, S. Liang, B. Shraiman, and C. Tang, Rev. Mod. Phys. **58**, 977 (1986).
[2] L. Patterson, Phys. Rev. Lett. **52**, 1621 (1985).
[3] D. Mader, *Hydraulic Proppant Fracturing and Gravel Packing* (Elsevier, New York, 1989).
[4] H.H. Hardy, Math. Geology **24**, 73 (1992).
[5] R. A. Beier (unpublished).
[6] J.S. Langer, Science **243**, 1150 (1989); in *Chance and Matter*, Proceedings of the Les Houches Summer School, Session 46, edited by J. Souletie, J. Vannimenus, and R. Stora (North-Holland, Amsterdam, 1986); D. Kessler, H. Levine, and J. Koplik, Adv. Phys. **37**, 255 (1988); in *Dynamics of Curved Fronts*, edited by P. Pelce (Academic, New York, 1988).
[7] M. Rabaud, S. Michalland, and Y. Couder, Phys. Rev. Lett. **64**, 184 (1990).
[8] V. Hakim, M. Rabaud, H. Thome, and Y. Couder, *New Trends in Nonlinear Dynamics and Pattern-Forming Phenomena* (Plenum, New York, 1989); M. D. Savage, J. Fluid. Mech. **80**, 743 (1974); *ibid.* **80**, 757 (1974); H. Cummins, L. Forture, and M. Rabaud, Phys. Rev. E. **47**, 1727 (1993).
[9] T. Witten and L. Sander, Phys. Rev. Lett. **47**, 1400 (1981).
[10] T. Halsey and M. Leibig (unpublished).
[11] J. Chazaviel, V. Fluery, and M. Rosso (unpublished).
[12] G. Kahanda, X. Zou, R. Farrell,and P. Wong, Phys. Rev. Lett. **68**, 3741 (1992).
[13] P. Wong, Phys. Today **41** (12), 24 (1988).
[14] D. Smith, X. Wu, A. Libchaber, E. Moses, and T. Witten, Phys. Rev. A **45**, R2165 (1992).
[15] F. Spaepen, Acta Metall. **23**, 615 (1975).
[16] E. Lemaire, P. Levits, G. Daccord, and H. Van Damme, Phys. Rev. Lett. **67**, 2009 (1991).
[17] H. La Roche, F. Fernandez, M. Octavio, A.G. Loeser, and C. Lobb, Phys. Rev. A **44**, R6185 (1991).
[18] D. A. Kurtze and D. C. Hong, Phys. Rev. Lett. **71**, 847 (1993); see also H. Zhao, J. Ignes-Mullol, and J. V. Maher, Bull. Am. Phys. Soc. **39**, 259 (1994); see also D. C. Hong and S. Yue, Phys. Rev. Lett. **74**, 254 (1995).
[19] B. Shraiman, Phys. Rev. Lett. **56**, 2028 (1986); D.C. Hong and J.S. Langer, Phys. Rev. Lett. **56**, 2032 (1986); Phys. Rev. A **36**, 2325 (1987); R. Combescot, T. Dombre, V. Hakim, Y. Pomeau, and A. Pumir, Phys. Rev. Lett. **56**, 2028 (1986).
[20] G.I. Taylor, Proc. R. Soc. London Ser. A **146**, 501 (1934).
[21] T. Dombre and V. Hakim, Phys. Rev. A **36**, 2811 (1987).
[22] D. Jasnow and J. Viñals, Phys. Rev. A **40**, 3864 (1989).
[23] H. Guo, D.C. Hong, and D.A. Kurtze, Phys. Rev. A **46**, 1867 (1992).
[24] R. Ball, *Statistical Physics* 16 (North-Holland, Amsterdam, 1986).
[25] L. Turchevich, and H. Sher, Phys. Rev. Lett. **55**, 1026 (1985).
[26] H. Guo, D.C. Hong, and D. Kurtze, Phys. Rev. Lett. **69**, 1520 (1992).
[27] W.W. Mullins and R. Sekerka, J. Appl. Phys. **3**, 444 (1964).
[28] P.G. Saffman and G.I. Taylor, Proc. R. Soc. London Ser. A **245**, 312 (1958).
[29] S. Chandrasekhar, Hydrodynamics and Hydrodynamic Stability (Dover, New York, 1961).
[30] P. Berge, Y. Pomeau, and C. Vidal, Order within Chaos (Wiley, New York, 1984).
[31] P. Manneville, Dissipative structures and weak turbulence (Academic, New York, 1989).
[32] A.R. Kopf-Sill and G.M. Homsy, Phys. Fluids **30**, 2607 (1987).
[33] J. Maher (private communication).
[34] E. Ben-Jacob, R. Godbey, N.D. Goldenfeld, J. Koplik, H. Levine, T. Mueller, and L.M. Sander, Phys. Rev. Lett. **55**, 1315 (1985)
[35] A.T. Dorsey and O. Martin, Phys. Rev. A **35**, 3989 (1987); see also D.A. Kessler, J. Koplik, and H. Levine, Phys. Rev. A **34**, 4980 (1986); D. C. Hong, Phys. Rev. A **43**, 5199 (1991)
[36] Y. Couder (private communication).
[37] A. Bhattacharjee and X. Wang, Phys. Rev. Lett. **69**, 2196 (1992).
[38] T. F. Duppont, R. E. Goldstein, L. P. Kadanoff, and S. Zhou, Phys. Rev. E **47**, 4182 (1993); **47**, 4169 (1993).